Advances in Colloid and Interface Science 288 (2021) 102341

Contents lists available at ScienceDirect

Advances in Colloid and Interface Science

journal homepage: www.elsevier.com/locate/cis

Historical Perspective

# Recent developments in emulsion characterization: Diffusing Wave Spectroscopy beyond average values

Valentina Lorusso [a,1], Davide Orsi [a,1], Fabrizia Salerni [a,1], Libero Liggieri [b], Francesca Ravera [b], Robert McMillin [c], James Ferri [c], Luigi Cristofolini [a,b,*]

[a] Department of Mathematical Physical and Computer Sciences, University of Parma, Parma, Italy
[b] Institute of Condensed Matter Chemistry and Technologies for Energy – CNR, Department of Genova, Italy
[c] Virginia Commonwealth University, Richmond (VA), USA

ARTICLE INFO

*Article history:*
30 October 2020
9 December 2020
10 December 2020
Available online 13 December 2020

*Keywords:*
Emulsions
Creaming and sedimentation
Diffusing Wave Spectroscopy-DWS
Optical Monte Carlo methods
Dynamical heterogeneities

ABSTRACT

We report here an overview of current trends and a selection of recent results regarding the characterization of emulsions by Diffusing Wave Spectroscopy (DWS). We provide a synopsis of the state of the art of the DWS technique, and a critical discussion of experiments performed on samples in which Brownian and ballistic dynamics coexist.

A novel analysis scheme is introduced for DWS experiments on creaming or sedimenting emulsions, allowing to extract not only average values for drop size and drop dynamics - as usual in DWS - but also properties related to the width of the distributions governing these quantities. This analysis scheme starts from a realistic Monte Carlo simulation of light diffusing in the volume of the sample and reaching the detector. This simulation is more accurate than the analytical expressions available for the idealized geometries normally used in DWS interpretation. By disentangling Brownian and ballistic motions we directly access the variance of velocity distribution, $\sigma_v$. In relatively unstable emulsions $\sigma_v$ governs the frequency of drop-drop collisions and subsequent coalescence events. Furthermore, when gravity dominates dynamics, as in emulsions subject to sedimentation or creaming, $\sigma_v$ is strongly related to the 2nd and 4th moments of drop size distribution.

This novel analysis scheme is exemplified investigating freshly formed model emulsions. Results are validated by comparison with microscopy imaging. This analysis is then extended to emulsions with a much broader drop size distribution, resembling those that are planned to be investigated in microgravity by the Soft Matter Dynamics facility onboard the International Space Station (ISS).

This review is concluded by sketching some promising directions, and suggesting useful complementarities between DWS and other techniques, for the characterization of transient regimes in emulsions, and of destabilization processes of great practical importance.



**Contents**



* Corresponding author at: Department of Mathematical, Physical and Computer Sciences, University of Parma, Parco Area Scienze 7/A, 43124 Parma, ITALY.
*E-mail address:* luigi.cristofolini@unipr.it (L. Cristofolini).
[1] These authors contributed equally to the work.

https://doi.org/10.1016/j.cis.2020.102341
0001-8686/

## 1. Introduction

Emulsions are mixtures of immiscible liquids, one of which is dispersed in the form of small drops into the other. Emulsions are widespread in nature, many synthetic products are emulsions, and many industrial processes rely on emulsification and emulsion stability. Therefore, their control is at the core of a wide range of technologies, from food to pharmaceutical and cosmetics industries, to oil extraction and water purification. The features of emulsions depend on properties related to drop size and dynamics, mostly controlled by surfactants. Emulsions are unstable, since the process of phase separation is energetically favoured, and density differences between the components induce creaming or sedimentation, but kinetic stability over long time can be ensured by suitable surfactants. These adsorb spontaneously at the drops interface, where their accumulation significantly alters the physico-chemical features. Surfactants also facilitate the production of emulsions, since they decrease the interfacial tension between the liquid phases, which is in fact proportional to the mechanical work needed to create new liquid-liquid interface. An ideally stable emulsion is characterized by a spatially uniform volume distribution of the drops in the continuous phase, and by a drop size distribution constant over time.

Although based on some general principles, emulsion formulation still relies on semi-empirical approaches. We lack in fact quantitative models predicting accurately the features of emulsions from properties of the surfactant layer at drop interface, which would be beneficial for a sustainable use of resources and to mitigate environmental impact of goods production and waste disposal.

Therefore, analytical techniques able to address emulsion stability and their mechanical properties are quite useful. Among these, Diffusing Wave Spectroscopy (DWS) is a correlation spectroscopy extending the domain of Dynamic Light Scattering (DLS) to turbid samples, such as foams and emulsions [1–6]. The principle behind DWS is the detection of temporal intensity fluctuations of coherent light from a laser, once it has been multiply scattered by the turbid sample. One attractive feature of DWS is that it is non-invasive, being based on all-optical detection. Furthermore, a typical DWS experimental setup is relatively simple and robust. For this reason, DWS is well suited to be implemented and employed in difficult environments such as that of microgravity experiments, to be performed onboard the International Space Station (ISS). As a matter of fact, DWS has already been implemented as the main diagnostics of the ESA *Soft Matter Dynamics* (SMD, formerly *Foam C*) facility, onboard the ISS, to perform experiments on emulsions, granular materials and foams.

The rest of the manuscript is organized as follows: we start by reviewing the processes governing emulsion evolution and the gravity driven dynamics of droplets, then we introduce the basics of the DWS technique, with special regard to the case of samples with an internal flow, to the use of Monte Carlo methods to describe light diffusion, and we review some selected results obtained by the application of this technique to emulsions. Next, we introduce a novel analysis scheme by which, in some cases, it is possible to extract not only average values for drop size and drop dynamics, but also the width of the distributions governing these quantities. This approach then is validated by a few experiments on model emulsions, for which we discuss the results, and the conclusions that can be drawn. Finally, we sketch a few directions that appear particularly promising for research in the near future.

### 1.1. The problem of stability in emulsions

An important feature in the design of fluid-fluid dispersions is stability. Typically, multiphase dispersions are thermodynamically unstable and tend to separate. Hence, the existence of kinetically stable dispersions relies on the presence of stabilizing agents. Stable emulsions are composed of small, uniform drops with a narrow and slowly evolving drop size distribution (DSD). Surface stabilizing agents are comprised of surface-active species, such as surfactants, proteins, and nanoparticles that adsorb at a fluid-fluid interface. This decreases the energy associated with the creation of interfacial area contravening destabilization. Now, consider the opposite process. Other additives (de-stabilizing agents) can be utilized to overcome the stabilizing effects of existing surface-active species – such as in natural emulsions - to destabilize and separate the fluid phases [7]. This is often referred to as emulsion breaking [8]. Though there has been numerous works investigating the role of surface-active species, much of the development and formulation of stabilizing or de-stabilizing models is still largely empirical.

As sketched in Fig. 1, different mechanisms contribute to emulsion destabilization, starting from those driven by gravity, namely sedimentation and buoyancy, which bring drops in close contact and facilitate aggregation, coalescence, and Ostwald ripening. These last processes increase drop size and may yield to phase separation. In the following, these are briefly revised:

1) The density difference $\Delta\rho$ between the drops and the continuous phase determines gravity-driven drifting, i.e. creaming or sedimentation of drops. The drift velocity $v$ is given by the balance of the shear stresses at the drop boundary [9]. At first approximation, neglecting hydrodynamic correlations and interfacial effects, this velocity is given by the well-known Hadamard-Rybczynski formula:

$$v = \frac{2\,R^2 \Delta\rho g}{3\eta}\left(\frac{\eta+\eta'}{2\eta+3\eta'}\right) \tag{1}$$

where R is drop radius, $\eta'$ and $\eta$ are the viscosities of the drop and of the continuous phase respectively and g is the gravity acceleration. For a typical drop of dodecane in water with radius $R = 5\ \mu m$, this amounts to $v \sim 16\ \mu m/sec$. This is a factor 1.16 faster than the Stokes velocity predicted for a solid sphere with the same size and density. This difference arises because of the internal flows present inside the drop - and absent inside a solid sphere - contributing to balance the interfacial shear stresses. The mechanical properties of the interface itself, related to the possible presence of an adsorbed layer, may also play a role. This was first introduced by Levich [10], and is discussed in the following section. Incidentally, we note the quadratic dependence of velocity from drop radius, which is common to all the models reported here. In real emulsions, whose drops size distributions are broad, this quadratic dependence makes velocity distributions even broader. This is an important point for the analysis of DWS results.

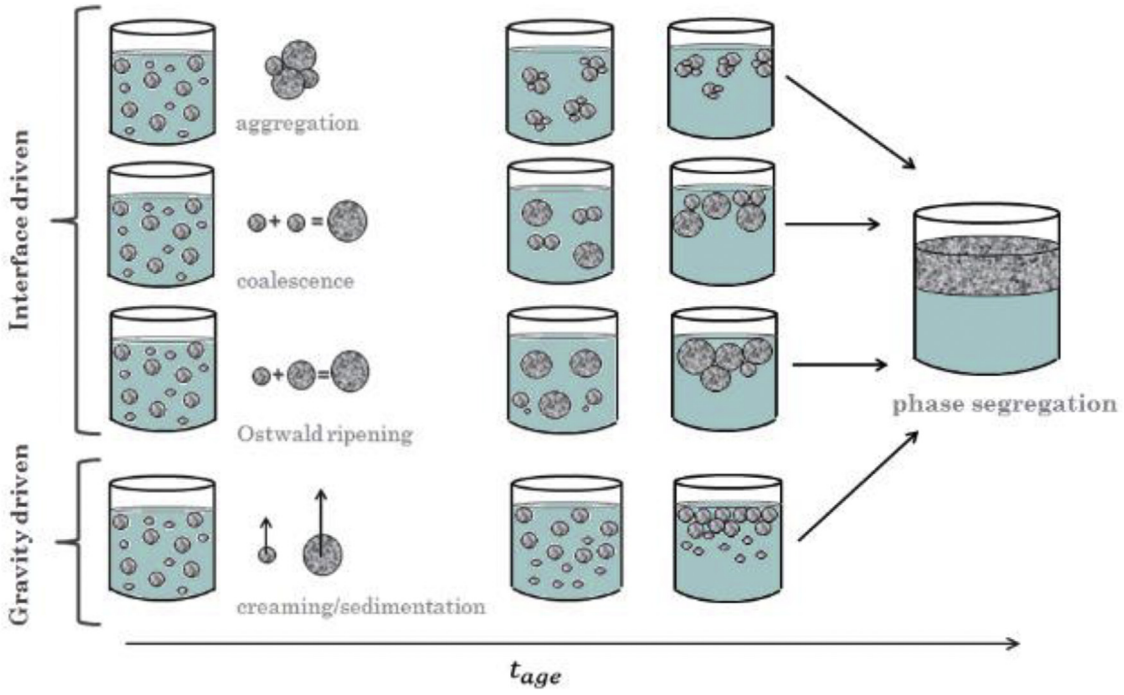


**Fig. 1.** Mechanisms determining emulsions destabilization: creaming, coalescence, and Ostwald Ripening.

Sedimentation or creaming in dense emulsions is also affected by hydrodynamic correlations. The motion of the drops induces a compensating backflow of the continuous phase, which reduces the average velocity of the drops because the continuous phase must flow through narrow channels between them. Together with this retarding effect, the opposite effect is also possible: the motion of each drop being affected by the particular configuration of its neighbours. Two close drops moving together move faster than if spatially separated because of the mutual drag mediated by the induced flow in the continuous phase. Quantifying these effects is one of the most difficult problems in hydrodynamics [11]. In the following we propose an experimental approach to quantify the root mean square of velocity differences for the drops of a creaming emulsion.

2) The dispersed phase (i.e. bubbles in foams or drops in emulsions) may form aggregates - either reversible or irreversible - where the drops are separated by a stable film of the continuous phase. The increasing size of aggregates results in their segregation by gravity and eventually in their phase separation. Aggregation occurs under the effects of the molecular interactions between two (or more) drops. This depends on the characteristics of the liquids, the surface active molecules, and on the thermodynamic state of the interface [12,13].
3) Larger drops, more prone to gravity segregation, can be formed after the spontaneous coalescence of smaller interacting drops, for example in aggregates. The coalescence phenomena are related to the stability of the film of matrix liquid between the drops [14]. The thinning of the liquid film can lead directly to rupture and drop coalescence, or to the formation of a stable film, as is the case for stable drop flocs. Thus, a key issue to hinder (or promote) emulsion destabilization is the thinning of the film and the physicochemical features of the surfactants or other stabilizing agents that underpin its formation [15,16]. Additionally, the interplay between the fluid dynamics of the emulsification process and the system physical chemistry, specifically the dynamic interfacial tension, $\gamma(t)$, and dilational interfacial viscoelasticity are also key factors [17–19]. The latter is the response of the interfacial tension to variations of the interfacial area and is related to the mechanical stability of the film when subject to external perturbation.
4) Larger drops grow at the expenses of the smaller ones under the effect of Ostwald ripening (OR) [20]. This is a non-equilibrium dynamic process driven by the difference of Laplace pressure between disparate-sized drops or bubbles [21]. Depending on the dispersed phase packing, the theory predicts growth of the drop or bubble size following a time-dependence: $t^{1/2}$ (concentrated emulsions) and $t^{1/3}$ (dilute emulsions) [22], arising from the limiting cases of diffusive exchange of dispersed phase molecules between the drops or bubbles occurring through the films between drops (or bubbles) or through the matrix bulk. The situation is more complicated for flocculated emulsions, due to the presence of both types of transport. Nonetheless, the interfacial tension, $\gamma$, plays a fundamental role in setting the driving force of the process, because the driving force for diffusion is the Laplace pressure, $\Delta P \sim \frac{2\gamma}{R}$ where $R$ is drop radius. Therefore, surfactants can retard or arrest OR. Practically, OR is usually slow, and its significance is limited to emulsions characterized by very tiny drops, of the order of 100 nm, or on very long timescales, encompassing several months if not years.

### *1.2. Corrections to creaming velocity due to interfacial effects, according to Levich*

The presence of surfactants adsorbed at the drop interface may affect the internal convective motion of drops, resulting in a retardation of the rising velocity, as compared to the Hadamard-Rybczynski law. In fact, the shear stress may set an inhomogeneous distribution of the adsorbed surfactant molecules, resulting by the sweeping of the surfactant molecules towards the drop pole opposite to the drop motion. The consequent Marangoni effect drags convection in the bulk of the drop. Further than on the bulk viscosities, the onset and intensity of this phenomenon depend on the capability of the system to counteract the adsorption gradients by in-layer and off-layer transport of surfactant,

and on the effects of these gradients on the interfacial tension. The former is mostly concerned with kinetic effects related to the surfactant interfacial and bulk diffusion, while the latter is concerned with the Gibbs Elasticity: $E_0 = -\partial\gamma/dln\Gamma$.

According to the early theoretical developments by Levich [10], a corrective factor is added to the Hadamard - Rybczynski relation (Eq. (1)) that becomes

$$v = \frac{2\,R^2\Delta\rho g}{3\eta}\left(\frac{\eta+\eta'+\kappa}{2\eta+3\eta'+3\kappa}\right) \tag{2}$$

where the parameter $\kappa$ accounts for the interfacial effects and depends on the features of the adsorption layer and of the processes involved in the balance of the adsorption gradients. In all cases, this relation predicts a value of $v$ smaller than predicted by the Hadamard-Rybczynski equation and approaches the value predicted by Stokes for a rigid sphere.

Levich considered different cases in his analysis. Particularly important in our context are those concerned with surfactants soluble in the continuous phase, where the attenuation of the adsorption gradients results in exchange of surfactant molecules between the interface and the bulk. Assuming such exchange to be diffusion-controlled, as it will be the case for most low-molecular weight surfactants, it is $\kappa = -\frac{2\delta}{3DR}E_0\frac{\partial\Gamma}{\partial c}$ where $\delta$ is the depth of the diffusion boundary layer around the drop, D the diffusion coefficient and c the concentration of the surfactant in the continuous phase.

Large absolute values of $\kappa$, typically associated with surfactant concentrations in the range ~$10^{-2} - 10^{-1}$* CMC, foster a solid-like behaviour of the moving drop/bubble caused by the immobilisation of the interfacial layer.

Modifications of the Levich theory have been further proposed, based on the concepts of rear stagnant cap (RSC), according to which, by effect of the drag exerted by the external liquid, the adsorbed surfactant is swept towards the rear of the drop [23]. According to the Levich concepts, a spherical cap around this pole may therefore present an immobilised interface and behave as a solid drop. The forward drop interface remains void from surfactants and the corresponding spherical cup respond to the drop motion according to the concepts at the basis of the H-R. The drop surface results fully immobilised above a critical amount of adsorbed surfactant, depending on its velocity and size.

It is important to underline that many studies [24,25] show that the surface of microscopic drops/bubbles can be immobilised even at very low surfactant concentrations, so that micrometric rising bubbles/drops behave as solid spheres. This can be rationalised on the basis of the RSC approach, that in fact predicts the minimum amount of adsorbed surfactant necessary to fully immobilise the drop interface as decreasing with the drop size [23,26]. For small bubbles/drops such adsorption is in addition extremely low. For a rising bubble of 100 $\mu m$, it was estimated [24] of the order of $10^{-9}$ $mol/m^2$, which, considering for example SDS adsorption layers, is determined by a bulk concentration well below what detectable by the current analytic or tensiometric techniques.

A complete review on the physicochemical aspects related to the drop motion is available in [27]. It must be however stressed that many complications are arising when concentrate sets of drops are considered. Therefore, the above sketched concepts apply only to emulsions characterized by relatively small volume ratio and large drops.

### 1.3. Diffusing Wave Spectroscopy (DWS)

Diffusing Wave Spectroscopy (DWS) [1,2] is a technique widely used to investigate both structure and dynamics in multiply scattering samples, such as emulsions. In DWS, coherent light from a laser source undergoes multiple scattering inside the sample before exiting and being detected. Autocorrelation functions are then calculated for the scattered light intensity $I(t)$. This can be done commonly in the homodyne regime: $g^{(2)}(t) = \frac{\langle I(t_0)I(t_0+t)\rangle}{\langle I^2\rangle}$ where the brackets $\langle\ldots\rangle$ refer to an average over initial time $t_0$, and in case of measurements based on multidetector (either a Charge Coupled Device, CCD or a Complementary Metal-Oxide Semiconductor, CMOS detector), also over space. In some cases, experiments are performed in the heterodyne regime, i.e. the light from the sample is mixed at the detector with a fraction of unscattered laser light. In this case, the measured quantity is the correlation function of the electric field $E(t)$: $g^{(1)}(t) = \frac{\langle \boldsymbol{E}(t_0)\cdot\boldsymbol{E}(t_0+t)\rangle}{\langle \boldsymbol{E}^2\rangle}$ where the brackets again indicate averaging. This correlation function is directly linked to the Intermediate Scattering Function $f(\boldsymbol{q},t)$, i.e. the spatial Fourier Transform of the van Hove Function $G(\boldsymbol{r},t)$ which encodes all the structure and dynamics of the sample. When the Gaussian approximation is satisfied, i.e. when many independently fluctuating volumes are probed, the two correlation functions are linked by the Siegert relation $g^{(2)}(t) = 1 + \beta g^{(1)}(t)^2$ - where the contrast $\beta$ depends on the geometry of the experiment [28].

The multiple scattering regime of DWS is different from Dynamic Light Scattering (DLS) and X-ray photon correlation spectroscopy (XPCS), which are based on single scattering events. Thanks to multiple scattering events, even if using visible light, DWS in transmission geometry allows accessing sub-nanometric displacements that would otherwise require X-ray techniques to be detected in the single-scattering regime. On the other hand, the statistical nature of this technique compromises the possibility to associate a single value of momentum $q$ to the observed dynamics, on the contrary, all scattering vectors between 0 and $2k_o$ contribute, where $k_o = \frac{2\pi m}{\lambda}$ is the light wavevector ($k_o \simeq 1.3 * 10^7 m^{-1}$ for radiation from a He—Ne laser propagating in water). However, the measured correlation function is determined by the Intermediate Scattering Function $f(\boldsymbol{q},t)$ weighted by $q^3$ average [1]. This implies that in most cases the dynamics observed in DWS can be safely attributed to the largest value of $q$ (i.e. $q_{DWS} \sim 2k_o$).

It is very instructing to think of the electric field at the measuring point as the (vectorial) sum of the fields arising through all the possible optical paths. In this case the relevant parameters are the path length $s$, and the corresponding statistical weight $P(s)$. For each path length, a partial $g_s^{(1)}(t)$ can be defined. Then the correlation function for the electric field $g^{(1)}(t)$ is expressed as the sum of all the partial contributions $g_s^{(1)}(t)$ each one weighted by the corresponding $(s)$:

$$g^{(1)}(t) = \int_0^\infty P(s)g_s^{(1)}(t)ds \tag{3}$$

Each contribution $g_s^{(1)}(t)$ can be expressed as an exponential decay due to the mean square displacement $\langle\Delta r^2(t)\rangle$ of the scattering centre over the time $t$, multiplied by the average number of scattering events corresponding to path length $s$, which is simply given by the ratio $\frac{s}{l^*}$, where $l^*$ is the transport mean free path, which will be discussed in the following.

$$g_s^{(1)}(t) = exp\left(-\frac{1}{3}\frac{s}{l^*}k_0^2\langle\Delta r^2(t)\rangle\right) \tag{4}$$

It is evident that, for a given system, longer paths decay faster than shorter ones, due to the larger number of contributions.

To model light diffusion in a DWS experiment as a random walk, based on *isotropic* scattering events, in Eq. (4) we have introduced the photon transport mean free path $l^*$. This is related to the distance $l$ between real scattering centres by the relation $l^* = l\frac{1}{\langle 1-cos\theta\rangle}$ where $\theta$ is the scattering angle, and $\langle 1 - cos\theta\rangle$ accounts for the bias of the real scattering. This, because the scattering in the Mie regime is biased with preferential forward direction and complete randomization requires more than one step of length $l$. In foams and emulsions, the combination of simultaneous experiments in backscattering and in transmission geometry on the same sample allows to determine the photon transport mean

free path $l^*$ which, under some hypothesis, can be shown to be proportional to drop size. We shall return on the quantification of this proportionality in the next section, devoted to Optical Monte Carlo simulations for the analysis of DWS results.

To use Eq. (3), the path length distribution (s) must be determined. Analytical formulas are available for some idealized geometries of the experiment: e.g. the cases of impinging laser beam focalized in a single point, or a uniform plane wave, and of detection either on the same side of the illumination (Backscattering, BS) or on the opposite side (Transmission, T). For a sample made of an infinitely extending slab of thickness $L$, with Brownian dynamics of characteristic time $\tau$, subject to uniform illumination, analytical formulas are the following (eq. 16.39b [1] and Eq. (4) from [2]):

$$g_T^{(1)}(t) = \frac{\left(\frac{L}{l^*}+\frac{4}{3}\right)\sqrt{\frac{6t}{\tau}}}{\left(1+\frac{8t}{3\tau}\right)\ sinh\left(\frac{L}{l^*}\sqrt{\frac{6t}{\tau}}\right)+\frac{4}{3}\sqrt{\frac{6t}{\tau}}\ cosh\left(\frac{L}{l^*}\sqrt{\frac{6t}{\tau}}\right)} \tag{5}$$

$$g_{BS}^{(1)}(t) = \frac{L}{L-\gamma l^*}\ \frac{sinh\left(\left(\frac{L}{l^*}-\gamma\right)\sqrt{\frac{6t}{\tau}}\right)}{sinh\left(\frac{L}{l^*}\sqrt{\frac{6t}{\tau}}\right)} \tag{6}$$

In which the phenomenological parameter $\gamma$ is introduced to describe the photon diffusion process as originating from a depth $\gamma l^*$ inside the sample.

An interesting application of DWS is in the field of rheology, where it extends the temporal domain towards high frequencies inaccessible to the normal rheology. The mean square displacements $\langle \Delta r^2(t) \rangle$ of the scattering centres can be related, by application of generalized Stokes-Einstein relations, to obtain creep compliance $J(t)$ and the mechanical viscoelastic moduli [1]. In the absence of any externally applied mechanical stress, $J(t)$ is directly proportional to the mean square displacement: $J(t) = \frac{\pi a}{k_B T}\langle \Delta r^2(t) \rangle$. From the compliance, the complex mechanical shear modulus $\widetilde{G}(\omega)$ is either obtained via Laplace transforms [29] or operating in the Fourier domain [30]. In the latter case,

$$\widetilde{G}(\omega) = G'(\omega) + iG\}(\omega) = \frac{1}{i\omega J(\omega)} \tag{7}$$

where $J(\omega)$ is the Fourier transform of $J(t)$ at the angular frequency $\omega$. The real part of $\widetilde{G}(\omega)$ is the elastic modulus $G'(\omega)$, while the imaginary part is the loss modulus $G''(\omega)$.

However, in dense emulsions it has been recently pointed out by Kim and co-authors [31] that it is necessary to take into account crowding effects which might alter the results by a considerable factor. This shall be discussed in more detail in a following section.

### 1.4. Samples with an internal flow

Systems in which an ordered flow of matter coexists with Brownian motion of individual particles are quite common, including soot particles in flames, aerosols, particle suspensions and emulsions subject to externally induced flow, to convective flow, or to gravity-driven sedimentation or creaming. Since their origin, light scattering spectroscopies have been applied to characterize these systems. The motion at constant velocity is often called "ballistic" in the corresponding literature.

Let us start by analysing the simplest case of light undergoing a single scattering event before detection, i.e. Dynamic Light Scattering (DLS). In this case it is known - see e.g. the fundamental textbook by Berne and Pecora [28] - that direct measurement of flow velocity is possible when experiments are performed in heterodyne mode, as long as the velocity $\boldsymbol{v}$ has a nonzero component along the exchanged momentum $\boldsymbol{q}$: an oscillating term, originated by Doppler shift, modulates the decay of the correlation function, which in case of coexisting ballistic and Brownian motion becomes $g^{(1)}(q,t) \propto \exp(-q^2 Dt)\cos(\boldsymbol{q}\cdot\boldsymbol{v}\,t)$ where D is the diffusion coefficient. Besides this, in a classical paper, Chowdury and co-authors [32] discussed the effect of the transit of the scattering centres entering and exiting the finite volume probed. If this scattering volume is defined by a gaussian sphere of waist $w$, which is a reasonable assumption for many experimental geometries, then the heterodyne correlation function is modulated by a gaussian term $\exp(-v^2t^2/2w^2)$, independently from the mutual orientation of velocity and exchanged momentum. The same factor also modulates the homodyne correlation function. Therefore, transit effects probe sample velocity independent of its orientation, for both homodyne and heterodyne detection, within the accuracy provided by the waist $w$. It is tempting to reduce $w$ to enhance sensitivity, however an additional non-Gaussian term appears in $g^{(2)}$, due to the fluctuation in the number of scattering centres in the probed volume, which become relevant in case of largely diluted systems or of extremely small volumes.

For the case of DWS, in which light undergoes a large number of scattering events before being detected, Wu, Pine, Weitz [33] show that DWS is sensitive to velocity differences inside the sample, which are able to vary the relative phase differences in the multiply scattered light. In particular, they show that when Brownian motion coexist with shear flow, all DWS correlation functions keep the same analytical form calculated in the classical case of pure Brownian motion, with the simple substitution of the term linear in time with the sum of one linear term and one quadratic in time:

$$\frac{t}{\tau_B} \rightarrow \left[\frac{t}{\tau_B}+\left(\frac{t}{\tau_S}\right)^2\right]$$

in which $\tau_B = D^{-1}k_0^{-2}$ is the usual Brownian relaxation time, related to the diffusion coefficient $D$, and $\tau_S$ is the shear decay time, related to the shear rate $\Gamma$ present in the sample by the relation:

$$1/\tau_S = \frac{\Gamma \cdot k_0 \cdot l^*}{\sqrt{30}} \tag{8}$$

where the numeric factor $\sqrt{30}$ comes from integration over unity sphere and normalization. This model was validated by DWS experiments on a suspension of latex particles dispersed in fluid undergoing laminar flow in Couette geometry. Subsequently, Bicout and co-authors [34,35] measured DWS in a variety of flow conditions, encompassing planar Couette flow as an example of homogeneous flow, planar Poiseuille flow as example of inhomogeneous gradient and Taylor-Couette instability. Their results prove that, in those conditions, DWS correlation functions are not influenced by mean velocities flow, but rather by the root mean square of velocity gradient. In well-defined geometries, for which the profile of velocity is known, DWS can also be used to quantify total flow, as demonstrated by Skipetrov and co-authors in [36]. The same Authors used then DWS to monitor blood flow, and the results are correlated with blood volume and oxygenation measured separately [37].

In general, transit effects are negligible in DWS, at difference with DLS. However, in a limit case Uhomoibhi and Earnshaw [38] demonstrated some transit effects in DWS in the case of a sample with no internal dynamics, namely Teflon tape of 0.570 mm thickness subject to uniform translation at controlled velocity, in the range up to 0.90 mm/s. In this case, the time evolution of $g^{(1)}(t)$ contains a gaussian decay which depends on the velocity and can be related to the time it takes to a typical coherence area to transit in and out of the detection area. In this experiment then DWS probes the *mean* velocity of the sample, and not velocity differences. It must be underlined however that this only happens because any other source of signal decoherence has been suppressed in this sample with no internal dynamics. Except this

case, and similar limit cases as a hypothetical emulsion subject to high speed jetting, in all common cases it remains true that DWS probes only *relative* motions of the scattering centres inside the sample.

We experimentally verified this with simple DWS experiments, in which the sample was rigidly translated in the vertical direction at constant velocities up to 143 $\mu m/sec$. The sample was a model suspension in water of polystyrene microparticles of size $d = 1\ \mu$m. Given that polystyrene is almost isodense with water, gravity driven dynamics is excluded, and particles follow a purely Brownian motion with diffusion coefficient at room temperature $D \sim 4 \cdot 10^{-13} m^2/s$. As shown in Fig. S1 of the Supplementary Information, DWS correlation functions are totally unaffected by this rigid translation even at the maximum translation speed of 143 $\mu m/sec$. At this speed, in the time in which a particle diffuses a distance equal to its size, $\tau_{self} = \frac{d^2}{D} \tilde{2.3}\ sec$ all the scattering centres are rigidly translated by the much larger distance of 0.3 *mm*.

This result is not unexpected and proves if needed that in this range of velocities DWS probes relative displacement between scattering centres and not their rigid translation.

### 1.5. Optical Monte Carlo methods applied to the interpretation of DWS results

Optical Monte Carlo methods are sparingly applied to DWS, where the literature, with a few exceptions, is mostly of experiments analysed with the analytical formulas derived for photon propagation in the well-defined geometries of illumination by infinite plane waves or by point sources, and the sample is assumed to be an infinitely extending slab of thickness L. One possible reason for this is that when DWS was founded (end of 80's and 90's) Monte Carlo Methods were less common than nowadays, mainly because of the limited computing power available, but also because in the Physics community, a closed analytical solution is always preferred to a "more dirty" numerical simulation. In the case of DWS however this might yield to the application of elegant models which do not completely describe the necessarily finite sample size. In particular, there is a trade-off between the requirement for a sample thickness $L$ much larger than the photon transport length $l^*$, necessary for the application of the analytical formulas and the limited sample thickness necessary to have a fair transmittance $T$ through the sample ($T \sim \frac{5}{3}\frac{l^*}{L}$) [1]. Furthermore, often overall sample size is limited because of experimental constraints, as is indeed the case for the microgravity experiments to be conducted with the 'Soft Matter Dynamics' facility onboard the International Space Station ISS. In all these cases, numerical simulations to determine the distribution of path length can be very useful.

A general and relatively recent review of Optical Monte Carlo methods can be found in [39], in which Doronin and co-workers discuss models of propagation of coherent polarized light, and their implementation on NVIDIA Graphics Processing Units (GPU) to take advantage of parallelization.

An interesting example of the application of Monte Carlo ray tracing specialized to DWS is reported in a classical paper by Crassous [40], who simulated light propagation and scattering in a random packing of identical spheres using a ray tracing algorithm, based on Fresnel and Snell laws. He has been able to demonstrate a proportionality relation between sphere radius and photon transport mean free path $l^*$. The proportionality factor is solely dependent on the mismatch $m$ between refractive index of the continuous phase and that of the spheres.

Basing on this result, in emulsions it is common to infer the drop radius from the DWS measurement of $l^*$. This measurement is easily done by combining a couple of simultaneous experiments of DWS in backscattering and in transmission geometry on the same sample. In the case of interest for the present work, dodecane in water emulsions at $T = 20\ ^\circ C$, probed by $\lambda = 633\ nm$ red light, the mismatch number $m$ turns out to be close to 1, due to the close values of the refractive indexes of dispersed and continuous phases, which makes the proportionality factor quite large. In these conditions, care must be paid to the control of temperature and of chemical purity, as a small variation of refractive index can have a large impact on the proportionality factor and hence on the apparent drop radius.

The appealing feature of this measurement is that it automatically yields a result averaged over the bulk of the emulsion, as opposed to direct observation by microscopy which normally focuses on drops either sticking or close to the container wall, which can be affected by many different factors and not resemble the real population. However, it is important to note that this link between $l^*$ and drop radius relies on some hypothesis not always fulfilled:

1) The calculation is performed for a system consisting of spheres all the same size. Therefore, at best, only an average value can be determined for drop radius. The width of the drop size distribution, or even the possibility of multimodality, are not considered and there is no direct way of obtaining a direct measurement of these. Moreover, when the width of the size distribution is important, one has to keep in mind that the measured average radius is an "optical average" i.e. it is weighted by the size-dependent scattering cross section of each drop, which in some case can be evaluated according to Mie. Opposite to most studies performed on model emulsions consisting of monodispersed size drops, real emulsions are characterized by a broad drop size distribution.
2) The assumption of a dense packing of spheres holds true only for the denser emulsions. Particularly in microgravity, or in density matched emulsions, the case can be given of long-lasting emulsions consisting of sparsely dispersed drops. In this case, not only drop radii, but also inter-drops separation distances both contribute to the determination of the length $l^*$, whose interpretation in terms of drop radius is then questionable.

In some cases, it can be desirable to vary continuously the distribution of path lengths. To this aim, Fahimi and co-authors [41] proposed to perform DWS experiments in a standard, variable angle goniometric DLS setup employing a cylindrical cuvette. Then for the interpretation of the results, they resorted to Monte Carlo simulations.

Having said that the examples of application of Monte Carlo methods to DWS are scarce, on the contrary, it must be emphasized that this approach is more widely applied in recent literature devoted to biological applications of correlation spectroscopies in the multiple scattering regime.

Optical Monte Carlo ray tracing has been applied to extend DWS to samples not fulfilling the classical requirements for this technique, either because of limited scattering or because of large absorption. The latter case is particularly relevant to biomedical applications, dealing with tissues absorbing light. The application of Monte Carlo ray tracing is described by Hajjarian and Nadkarni [42] in the interpretation of the results from a technique similar to DWS called Laser Speckle Rheology (LSR) that aims at measuring the viscoelastic properties by analysing the temporal fluctuations of backscattered speckle patterns, in particular of biological fluids. Depending on the concentration of scattering centres, this technique resembles DWS or DLS with detection at 180°. This crossover is phenomenologically described by a generalization of the expression for the intensity correlation function which takes a stretched exponential form $g^{(2)}(t) = 1 + e^{-2\gamma(k_0^2 n^2 \langle \Delta r^2(t) \rangle)^\zeta}$ governed by the stretching parameter $\zeta$ and a prefactor $\gamma$. These phenomenological parameters can be estimated by the Monte Carlo methods. They always take intermediate values between the limiting cases of DLS ($\gamma = \frac{2}{3}; \zeta = 1$) and DWS ($\gamma = \frac{5}{3}; \zeta = \frac{1}{2}$). Thus, this work indicates that the approach of Monte-Carlo ray tracing reliably compensates for any arbitrary optical variations in case of moderate scattering. Also the effect of light absorption can be accounted, as shown in another paper by the same authors, which show that in the case of moderate absorption, the standard DWS analysis can be implemented successfully to obtain viscoelastic moduli [43].

Similar Monte Carlo photon transport simulations have also been applied by Brake and co-authors [44] to describe the dependence of DWS relaxation times on the thickness of a biological sample, with application to the analysis of slices of soft tissues (rat brain).

### 1.6. Recent results on emulsions obtained by DWS

Real emulsions are very complex systems, in which many types of dynamics might simultaneously occur. Starting from an isolated drop, its simplest dynamics is due to thermally induced shape fluctuations. The extra area $\Delta A$ created by such fluctuations can be estimated to be of the order of $\Delta A \frac{\tilde{k_B T}}{\gamma} \tilde{4}0\ A^2$ for a typical value of $\gamma \sim 10$ mN/m. For a typical drop of radius 1 $\mu m$, this amounts to a relative variance of the mean radius of just $10^{-7}$. Furthermore, the viscosity of the dispersed phase implies that these fluctuations decay in a time of the order of 1 $\mu s$.

Despite their small amplitude and fast decay, drop-shape fluctuations are detectable by DWS; their effects in DWS have been modelled first by Gang, Krall and Weitz [45]. These authors showed that the corresponding contribution to $g^{(1)}(t)$ is decoupled from that due to translational diffusion, to which it is summed in the argument of the exponential.

Very recently, Yoon and co-authors [46] performed a clever experiment to quantify this contribution. They employed an emulsion formed by a wax, measured by DWS a few degrees above and below its melting temperature, thus effectively turning on and off these fluctuations in an otherwise almost constant system. Clearly, shape fluctuation must be considered especially when evaluating mean square displacement of the drops at early times, e.g. in the analysis to extract the mechanical moduli (Eq. (7)).

Besides individual drop dynamics, also correlation between the dynamics of adjacent drops can be very important. Braibanti and co-authors [47] investigated dense emulsions choosing a model system made by a concentrated silicone oil-in-water nanoemulsions, where the range of the soft repulsive interactions are tuned simply varying ionic strength. By DWS integrated with DLS experiments performed in a regime of controlled low coherence to limit multiple scattering, they obtained correlation functions and Intermediate Scattering Functions over a wide regime of concentrations and timespans. This allows to identify four distinct dynamical regimes at increasing concentration 1) a liquid and supercooled near-glassy regime, 2) a glassy regime, 3) an electrostatically jammed regime, corresponding to a significant overlap of the Debye layers, and, 4) an interfacial jammed regime. Notably, DWS was applied both in heterodyne and in homodyne mode, i.e. with and without a fraction of the impinging beam used as a local oscillator, to cover the smaller displacements found in the arrested states.

The same correlations in concentrated emulsions also affect the apparent mean square displacement (MSD) of the drop positions, which is used to calculate the frequency dependent mechanical viscoelastic modulus $\tilde{G}(\omega)$ by means of Generalized Stokes Einstein relations. Kim, Mason and co-authors [31] investigated the low-frequency plateau elastic shear moduli $G_0$ of concentrated, monodisperse, disordered oil-in-water emulsions as drops jam and demonstrate that collective scattering significantly affects the apparent MSD $\langle \Delta r_a^2(t) \rangle$ observed by DWS in dense colloidal emulsions. To simplify the analysis, drop internal dynamics is suppressed by using a high viscosity oil (PDMS). As a function of the oil fraction $\phi$, for growing crowding, they find significant corrections to the transport mean free path $l^*$ computed in the independent scattering approximation (ISA). This leads to introduce a $\phi$ dependent structure factor

$$\langle S_\phi(q) \rangle = \frac{l^*_{ISA}}{l^*} \tag{9}$$

This is then employed to extract the true MSD of the drops from the $\langle \Delta r_a^2(t) \rangle$ obtained by the standard procedures normally employed to analyse DWS c.f. via $\langle \Delta r^2(t) \rangle = \langle S(q) \rangle \langle \Delta r_a^2(t) \rangle$ where the average over $q$ is performed over the whole range up to $2k = 4\pi n/\lambda$. Their main result is that the true MSD is smaller by a sizeable factor, up to 2, than the apparent value obtained by DWS e.g. for $\phi = 0.5$. With this correction, excellent quantitative agreement is found between the elastic modulus measured by macro rheology and the elastic plateau deduced by DWS analysis. This result implies that such structural correction needs to be always calculated when mechanical modulus is to be extracted by DWS in concentrated emulsions.

Orsi and co-authors [5], also in view of future experiments on emulsions to be performed in microgravity conditions, onboard the International Space Station, quantified the accuracy of DWS correlation functions, either obtained by cross correlation of the signal from a couple of detectors, or from multipixel detectors such as linecameras. This aspect requires particular care as non-independent information are combined to form the correlation function, both because of temporal correlation and of possible spatial correlations when large coherence areas are oversampled by more than one detector. The results have then been validated by comparison with the variance of correlation functions from repeated measurements. This helps to set the temporal or frequency limits of the accurate determination of the mechanical moduli, providing an objective criterion to establish the time window over which DWS results are reliable, going beyond the "rule of thumb" that DWS is reliable on the time window on which the correlation function effectively evolves departing from the initial plateau and before reaching its long-time baseline.

This was later employed to offer a consistent picture of the phenomenology and of the mechanisms destabilizing a paradigmatic oil-in-water emulsion formed by dodecane in water and stabilized by SDS in the regime of low surfactant content. It has been shown that after creaming, these emulsions reach slow ageing regimes in which oil drops undergo local diffusive rearrangements only at early times, and the drop motion becomes caged at longer times. Correspondingly, the mechanical modulus is approximately viscous above a threshold of angular frequency $\simeq 10\ rad/s$, while it is deeply viscoelastic at lower frequencies. As ageing proceeds, this phenomenology does not change, but mechanical modulus rigidly shifts to higher values following a power law of ageing time, with a weak time dependence characterized by an exponent $\alpha \simeq 0.20$ independent of [SDS] concentration. This can be explained in terms of progressive drainage of water and slowly increasing packing of the drops.

Interestingly, in this ageing regime, the DWS relaxation time strongly depends on the [SDS] concentration, with a maximum around 2 $mM$, which is reminiscent of a similar dependence found for the dilational modulus $E_{dil}$ of the interface of a single drop, as measured by drop tensiometry experiments [16]. The relaxation of the DWS correlation function reflects the average response of the emulsion deriving from isolated or collective relaxation processes of drops. Being a response to a thermal excitation, they could be for example drop shape deformation or flickering, drop translations, coalescence between drops or Ostwald ripening. For emulsions stable for long time however it can be ruled out that the dynamic arises from any irreversible process, such as drop-drop coalescence or Ostwald ripening. Also, flickering of an isolated drop can be ruled out as too fast. A more plausible explanation can be hypothesized involving local perturbations of the adsorbed layer because of translation of drops. Thus, it can be assumed that the decay of DWS correlation functions in this model emulsion, in its strongly aged regime is presumably due to the displacement of the centre of mass of the drops and corresponding restoring forces due to the surfactant layer adsorbed at the oil-water interface.

Finally, to quantify and characterize drop-drop aggregation and coalescence events, for which the mean frequency or volumetric density values are negligibly small on average, higher order correlation functions are needed. An excellent review of DWS on emulsions and foams by Hohler and co-authors [48] has the merit of focusing on the characterization of dynamical heterogeneity, either spatial and temporal, by

employing a multidetector, and applying concepts of time resolved correlation spectroscopy and of speckle visibility [4,49]. While some interesting results have been obtained on foams, also thanks to the large size and large optical contrast of air bubbles, almost nothing is known in the case of emulsions, whose smaller drops typically present also smaller optical contrast between continuous and dispersed phases. This is a direction to be pursued in the near future.

## 2. Monte Carlo simulations of path length distributions $P(s)$ in real sample cells

For the quantification of creaming velocities, and of ballistic motion in general, it is necessary to reproduce with great accuracy the shape of DWS correlation functions, not only in terms of characteristic time but also of more or less steep shape. It is important to underline that also other factors might contribute to determine the steepness of the decay: namely optical absorption and finite size effects. The former induces an additional exponential decay to the path length distribution $P(s)$ thus reducing the relative weight of longer paths. The latter induces the same type of effect due to the geometrical cut-off of the longest paths, so that performing experiments in a confined geometry results in a more compressed shape of the correlation function, than that predicate for the infinite slab geometry. Thus, both geometric and absorption effects mimic the signature of ballistic motion.

In the case of the emulsions of our interest, we can rule out optical absorption, as absorption of light from dodecane, SDS and water are all negligible in the wavelength range used ($\lambda = 633nm$). On the contrary, geometrical effects can be important: the standard analytical formulas for the correlation functions measured in backscattering and transmission DWS [1] are derived under the strong assumption that photon propagation occurs in media of infinite lateral extension, and whose thickness $L$ is by far larger than photon transport length $l^*$. However, most experiments are performed in typical optical cuvettes of lateral sizes of about 1 *cm*, which does not fulfil these assumptions whenever $l^*$ exceeds typically 1 mm.

Therefore, experimental correlation functions need to be fitted by ones obtained using explicitly calculated path length distribution function $P(s)$ which can be generated via Monte Carlo simulations in the real geometry. We choose to do so in the Matlab computing environment, which is quite efficient by allowing implicit parallelization if the simulation is articulated in photon bunches. Optimal bunch size is of the order of $10^5$ photons with a typical Win10 64-bit running on 8 GB RAM. Many bunches are successively and independently generated to build up a statistical ensemble. The philosophy of the simulation is hence to follow photon propagation by a random walk process, keeping trace of the fate of each photon.

We choose a reference frame in which $X$ is the horizontal direction of the impinging laser beam, $Y$ is the other horizontal direction and $Z$ is vertical. At the initialization step, we define the cuvette size and two detection areas, one for backscattering and one for transmission experiments.

Initial positions for each photon are generated inside the sample, at a depth $l^*$, with lateral distribution in the $YZ$ plane either uniform or gaussian to account for these two possible beam profiles.

Then the core of the Monte Carlo algorithm consists in generating the directions of the steps uniformly distributed over the sphere, while the step lengths, following the approach of Durian and co-authors [50], follows a lognormal distribution with average value $l^*$, rather than being identically fixed to $l^*$. This choice has no effect in the results for transmission geometry but yields better reproduction of the analytically exact formulas for the correlation functions simulated for the infinite slab in backscattering geometry.

At each step, the fate of each photon is checked: if it is still inside the sample volume, the counter of the path length is incremented by one unit and the photon is retained for the next steps of the simulation. If on the contrary the photon has come out of the sample volume, simulation for this photon stops, and depending on whether this happened outside the measurement areas or inside one of them, the corresponding counter of the steps is discarded or retained in the appropriate (backscattering or transmission) pool. This corresponds to the absorbing confinement condition, which we choose as the most realistic reproduction of the real experiment.

When enough photons have been simulated, from the pool of path lengths recorded for the backscattering and the transmission geometries, the corresponding path length distributions $P(s)$ are generated and saved to a file. The process is then repeated for different values of $l^*$, to obtain the different $P(s)$ distributions to be used in the subsequent fitting procedure. The Matlab code employed for this Monte Carlo simulation is made publicly available on the Mathworks Central File Exchange platform [51]. The results have been validated also by comparison with the known analytical formulas (e.g. Eqs. (5) and (6)) for the classical geometries of the infinite slab of thickness much larger than $l^*$.

### 2.1. Fitting DWS correlation functions using simulated P(s)

To produce the model curves to fit the experimental correlation functions, we run sets of Monte Carlo simulations, obtaining path length distributions $P(s)$ for backscattering and transmission geometries, for different values of $l^*$ on a finely spaced comb covering a broad range of values, typically from one order of magnitude smaller to one order larger than the expected value. For the particular case reported here, the range is 0.1 to 10 *mm*.

These path length distribution $P(s)$, represent a static feature related to the internal structure of the sample. The dynamics is then introduced by the time dependence of the mean square displacement of the scattering centres, in the way it affects each of the partial contributions $g_s^{(1)}(t)$ to Eq. (3). Then $g^{(1)}(t)$ is obtained by trapezoidal integration of Eq. (3) and from this, $g^{(2)}(t)$ is calculated. For the common case of Brownian motion, this resorts to eq. 16.26 of [1], while for the case of ballistic motion, to Eq. (7) of [33].

In practice, the role of $l^*$ is to gauge the difference between the decays measured in Backscattering and in Transmission, and once the two are well determined experimentally, in the fitting $l^*$ is decoupled from the characteristic times $\tau_B$ and $\tau_S$, as well as from backgrounds and contrasts. In other words, their cross correlation is negligible. This allows a robust fitting procedure based on performing the best least squares fit for each value of $l^*$, and then choosing among these fits, the one with the lowest value of reduced $\tilde{\chi}^2$, defined as $\tilde{\chi}^2 = \sum_{T,BS} \frac{1}{N-P} \sum_{t_i} \left(\frac{g^{(2)}_{exp}(t_i) - g^{(2)}_{theo}(t_i)}{\sigma(t_i)}\right)^2$ where $g^{(2)}_{exp}(t_i)$ and $g^{(2)}_{theo}(t_i)$ are the experimentally measured and theoretically calculated correlation functions respectively, $\sigma(t_i)$ is the corresponding experimental uncertainty calculated as in [5], the sum is extended to the N values of times $t_i$ and to the two correlation functions measured in Backscattering (BS) and in Transmission (T), and P is the number of free fitting parameters. We recall that the reduced value of $\tilde{\chi}^2$ is close to 1 when the model describes adequately the data, while larger values of $\tilde{\chi}^2$ indicate that the model must be discarded. The best fit is calculated for each value of $l^*$ independently and the corresponding reduced $\tilde{\chi}^2$ is stored for future analysis.

We exemplify this approach in Fig. 2, reporting the analysis of correlation functions measured on an emulsion with $[SDS] = 4\ mM$ at $t_{age} = 10\ min$ after preparation; the sample was contained in a standard 1 *cm* cuvette. The correlation functions measured in backscattering (BS, red) and in transmission (T, black) are reported normalized to their respective backgrounds and contrasts. These are independently evaluated as the means of the short-time and long-time values of each correlation function, and are not fitting parameters in the model. These parts of

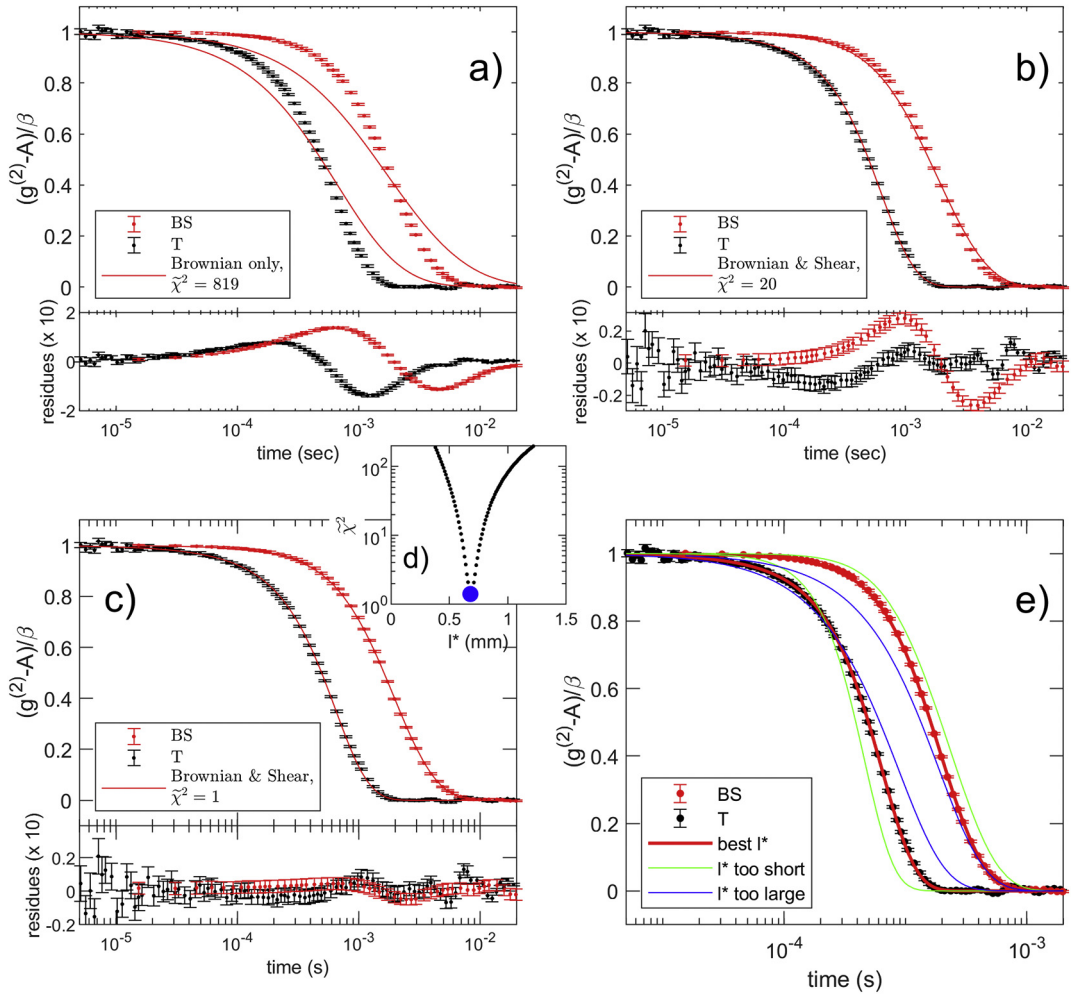


**Fig. 2.** DWS correlation functions measured in transmission (T, black points) and backscattering (BS red points) on a dodecane-in-water emulsion (50/50 volume ratio) stabilized by SDS surfactant (4 *mM*) at $t_{age} = 10$ *min*. Errorbars are deduced by the method reported in [5]. a) Fit with the classical analytical model of Eqs. (5) and (6), assuming purely Brownian dynamics; the very high value of $\tilde{\chi}^2$ and the residue plot (inset at the bottom) indicate that this model badly fails. b) Fit with an analogous analytical model, now including also ballistic motion. The agreement improves (see residue inset), but the fit is still not good ($\tilde{\chi}^2 = 20$). c) The fit is improved by considering the real shape of the sample, with Monte Carlo simulations of $P(s)$ for different values of the photon transport length $l^*$. The best fit yields $\tilde{\chi}^2 = 1.4$ and the plot of the residues confirms the agreement. Inset d) reduced $\tilde{\chi}^2$ of the fits for each value of $l^*$; the blue point indicates the minimum value $\tilde{\chi}^2 = 1.4$ which corresponds to $l^* = 0.68$ *mm* e) Representation of the effects of wrong values for $l^*$. Red lines are the best fits to the measured correlation functions, in green and blue are "wrong" fits: the model curves for BS and T are either too far apart (green, $l^*$*too short*) or too close to each other (blue, $l^*$ too large).

the correlation functions which have been used to determine baseline and contrast are excluded from further fitting.

We start evaluating the performance of the analytical model assuming sample shape to be an infinite slab and internal dynamics to be purely Brownian (Eqs. (5) and (6)). In panel a, we report this fit; the model clearly fails, with a ridiculously large value of reduced $\tilde{\chi}^2 = 819$. We then refine the model by including ballistic heterogeneous dynamics, encoded in the shear time $\tau_S$. As shown in panel b, this significantly improves the fit. However, the residues plot and the value of $\tilde{\chi}^2 = 20$ indicate that neither this model is adequate to describe the data.

A further improvement of the model can be obtained by including the effects of finite size of the cuvette, and of the detector, on the path length distribution $P(s)$. This is done via the Monte Carlo simulations described in the previous section. Panel c reports the best fit thus obtained; solid lines are the best fits, corresponding to the minimum value $\tilde{\chi}^2 = 1.4$. In panel d we show how the quality of the fit, measured by $\tilde{\chi}^2$, depends on the chosen value of $l^*$, which we recall is not a fitting parameter in this scheme of analysis. From this plot, we clearly identify the correct value of $l^*$ as the one yielding the minimum $\tilde{\chi}^2$. This approach is more robust than the alternative of treating $l^*$ as a fitting parameter subject to continuous variation, which would require interpolating $P(s)$ for intermediate values of $l^*$ hence potentially amplifying noise fluctuations unavoidably associated with the finite number of simulated photons over which $P(s)$ is calculated. For the sake of completeness, we report in panel e the effect of choosing an $l^*$ too short or too long: red lines are the best fits to the measured correlation functions, in green and blue are "wrong" fits: the model curves for BS and T are either separated too much (green lines, $l^*$ too short) or too close to each other (blue lines, $l^*$ too large).

We note that this type of analysis is only applicable when baseline and contrast can be well determined, otherwise their cross correlation with the shape of the decay and the characteristic times would make this analysis unreliable.

## 3. Results from the investigation of freshly prepared emulsions

### 3.1. Drop size distribution from microscopy imaging

Emulsions have been prepared following the procedure described in the Materials and Methods section of the Supplementary Information.

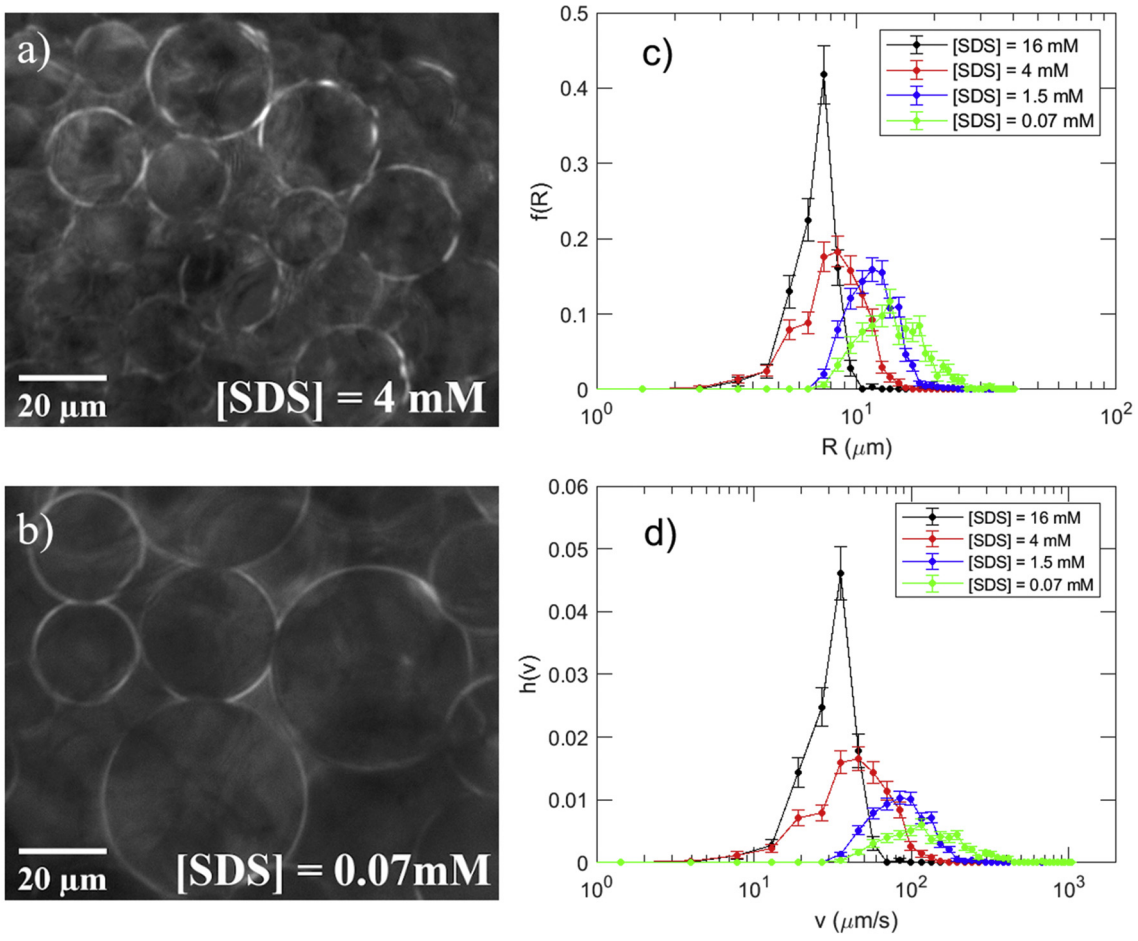


**Fig. 3.** Microscopy images showing individual drops from dodecane-in-water (50/50 volume ratio) emulsions stabilized by SDS in concentration [SDS] = 4 mM (panel a) and 0.07 mM (panel b). c) Distributions f(R) of drop radii of emulsions for different contents of surfactant, deduced from images of representative ensembles of at least 350 individual drops d) Distributions h(v) of creaming velocities, calculated according to Hadamard-Rybczynski Eq. (1) from the drop radii distributions f(R) of panel c).

**Table 1**
Results of microscopy measurements on freshly prepared dodecane-in-water (50/50 volume ratio) emulsions stabilized by different surfactant content. The table reports the values of mean radius ⟨R⟩ and standard deviation $\sigma_R$ calculated from distributions f(R) shown in panel c of Fig. 3, and mean velocity ⟨v⟩ and standard deviation $\sigma_v$ calculated from distributions h(v) shown in panel d of Fig. 3.

| [SDS] (mM) | $\langle R \rangle$ ($\mu m$) | $\sigma_R$ ($\mu m$) | $\langle v \rangle$ ($\mu m/s$) | $\sigma_v$ ($\mu m/s$) |
|---|---|---|---|---|
| 16 | 7.1 | 1.1 | 33.2 | 10.1 |
| 4 | 8.7 | 2.2 | 50.9 | 24.7 |
| 1.5 | 12.1 | 2.5 | 96.5 | 41.7 |
| 0.07 | 15.1 | 4.4 | 157.3 | 97.2 |

The drop size distributions were characterized by microscopy imaging on freshly prepared emulsions, always at $t_{age} < 10$ *min*. Details on the microscopy experiments can be found in the same Materials and Methods section of the Supplementary Information. Examples of the images obtained are reported in panels a and b of Fig. 3. The best estimate for drop radii distributions $f(R)$ have been obtained by drawing frequency histograms with a bin width of 1.0 $\mu m$, for representative ensembles consisting in a minimum of 350 individual drops. The results are reported in panel c of the same figure, on semi-logarithmic axis.

As [SDS] is reduced, emulsification produces larger drops on average; the width of the size distribution increases as well. In panel d of the same figure, we report the corresponding distributions of creaming velocities for these drop populations, obtained by the Hadamard-Rybczynski Eq. (1). Average values and standard deviations of distributions $f(R)$ and $h(v)$ for emulsions stabilized by different SDS content are reported in Table 1.

### 3.2. Results from Diffusing Wave Spectroscopy

DWS measurements were performed on fresh emulsions, and as a function of ageing time $t_{age}$; Transmission and Backscattering correlation function were simultaneously measured and are shown in the Fig. 4 for an emulsion stabilized by $[SDS] = 1.5\ mM$. To ensure reproducibility, for each of the compositions reported here the DWS experiments have been conducted in duplicate, more details regarding the DWS experiments are described in the Materials and Methods section of the Supplementary Information.

The correlation functions thus obtained are fitted by the model previously described, and schematized in Fig. 2. The outcome parameters are $l^*$, describing the structure, and the two characteristic times describing the dynamics, i.e. $\tau_B = D^{-1}k_0^{-2}$ describing Brownian motion with diffusivity $D$, and $\tau_S$ describing velocity differences in terms of a shear rate.

Let us start by the results on the internal structure of the emulsion. From the already cited approach of Crassous [40], neglecting drop size polydispersity, the average drop radius can be assumed to be proportional to $l^*$, with a proportionality factor given by the ratio of refractive indexes of the two liquids; in the case of dodecane-in-water emulsions, this ratio is $l^*/R = 86$ [6]. We recall that the width of the size distribution is inaccessible by this analysis.

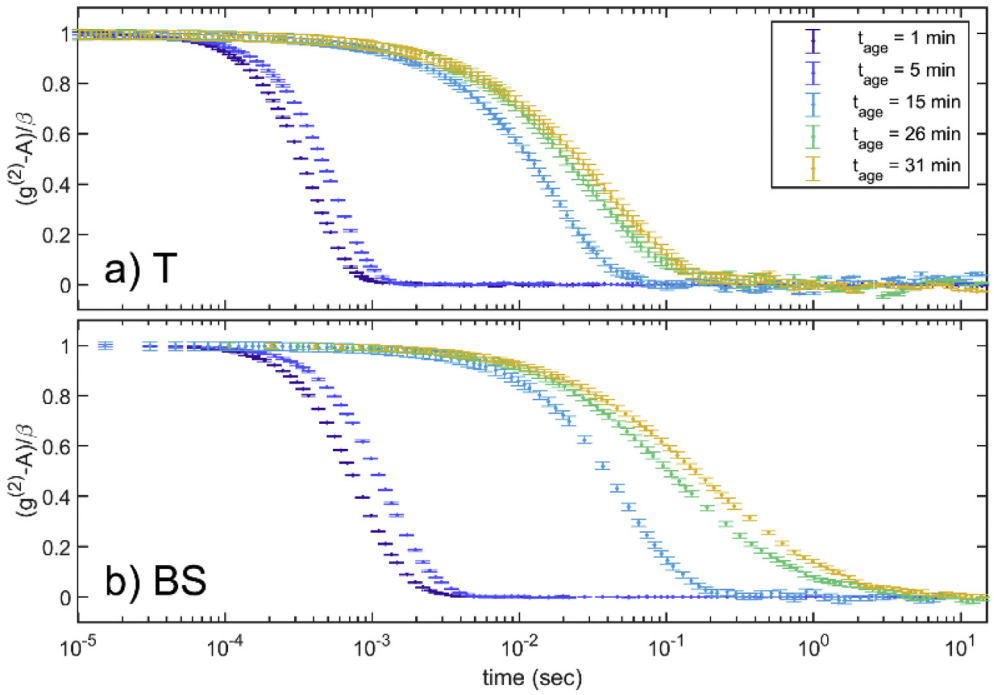


**Fig. 4.** DWS Transmission (T, panel a) and Backscattering (BS, panel b) correlation functions, simultaneously measured on a freshly prepared dodecane-in-water (50/50 volume ratio) emulsion stabilized by SDS at the concentration 1.5 mM. Correlation functions decay with a compressed shape at short ageing time; as the creaming process ends, the correlation functions decay more slowly and with a less steep shape, suggesting the transition from ballistic to Brownian dominated dynamics.

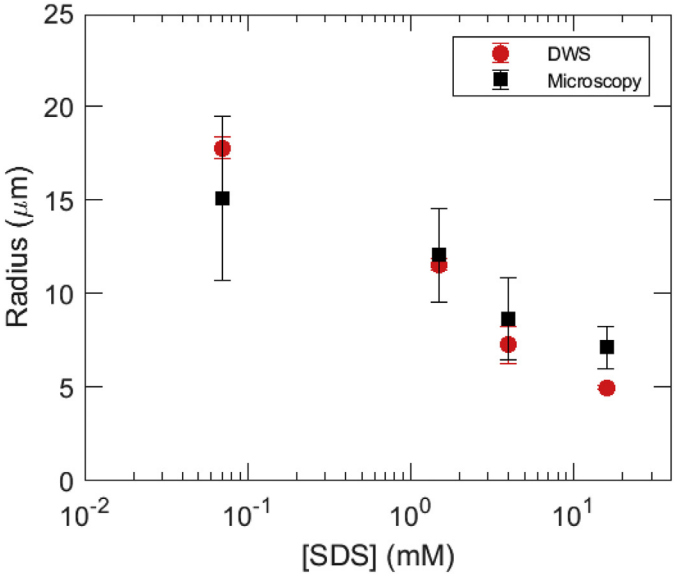


**Fig. 5.** Mean drop radius of freshly prepared emulsions as a function of [SDS], as deduced from the transport mean free path $l^*$ according to ray-tracing simulations [40] (red circles) and from direct microscopy observation (black squares). In the case of Microscopy, error bars represent the actual width of the drop radii distribution. In the case of DWS instead, the width of the distribution is not directly accessible, and the error bars are statistical uncertainties.

The effect of the concentration of SDS on the initial drop size is shown in Fig. 5, where the average radii obtained from DWS (red points) are compared to those obtained from microscopy (black points) for four emulsion of different SDS content. Error bars in the figure have two different meanings: for DWS they represent statistical uncertainty, while for microscopy they represent the widths of the distribution of radii seen by microscopy shown in Fig. 3.

Regarding the dynamics, Fig. 6 reports $\tau_B$ and $\tau_S$, at different ageing times $t_{age}$. At short $t_{age}$, during the creaming process, both Backscattering and Transmission correlation functions present a compressed exponential decay; correspondingly, we find $\tau_S \ll \tau_B$. As creaming progresses, $\tau_s$ increases; at the time $t_{age}$ where creaming process ends, we observe a crossover of the two relaxation times, and $\tau_S > \tau_B$; at this point, $\tau_S$ cannot be determined by the fitting routine.

## 4. Discussion

Let us start by analysing how the average values of drop radii depend on surfactant concentration in freshly prepared emulsions. As shown in Fig. 5, in this case the average drop radii grow for decreasing concentration in the deep submicellar regime. This contrasts with the results found for the same emulsions after several days of ageing in which we found a substantial independence of the average radius from surfactant from well below to above the critical micellar concentration [6]. This difference can be understood by observing that in freshly prepared samples, in particular for those with the lowest content of surfactant, the drop size distribution is broad and comprises both large and small drops as shown in Fig. 3 and summarized in Table 1. With time, as ageing proceeds, larger drops disappear because of creaming and of coalescence by the mechanisms mentioned in the introduction, thus leaving a less polydisperse distribution of smaller drops. This is an example demonstrating the importance of capturing the width of the distributions, and not only the average values, if one is to understand emulsion evolution and stability. The agreement between the mean drop radius determined by DWS and by microscopy, reported in Fig. 5, validates our DWS analysis. This agreement can only be expected in emulsions whose drop size distribution is not too broad, otherwise the size dependence of Mie scattering power would introduce a measurable effect in DWS.

Now let us consider the internal dynamics of emulsions. We turn our attention here in particular to the dynamics at early times, in which creaming cannot be neglected. In the literature of DWS on emulsions, this regime is often considered as a transient and not analysed

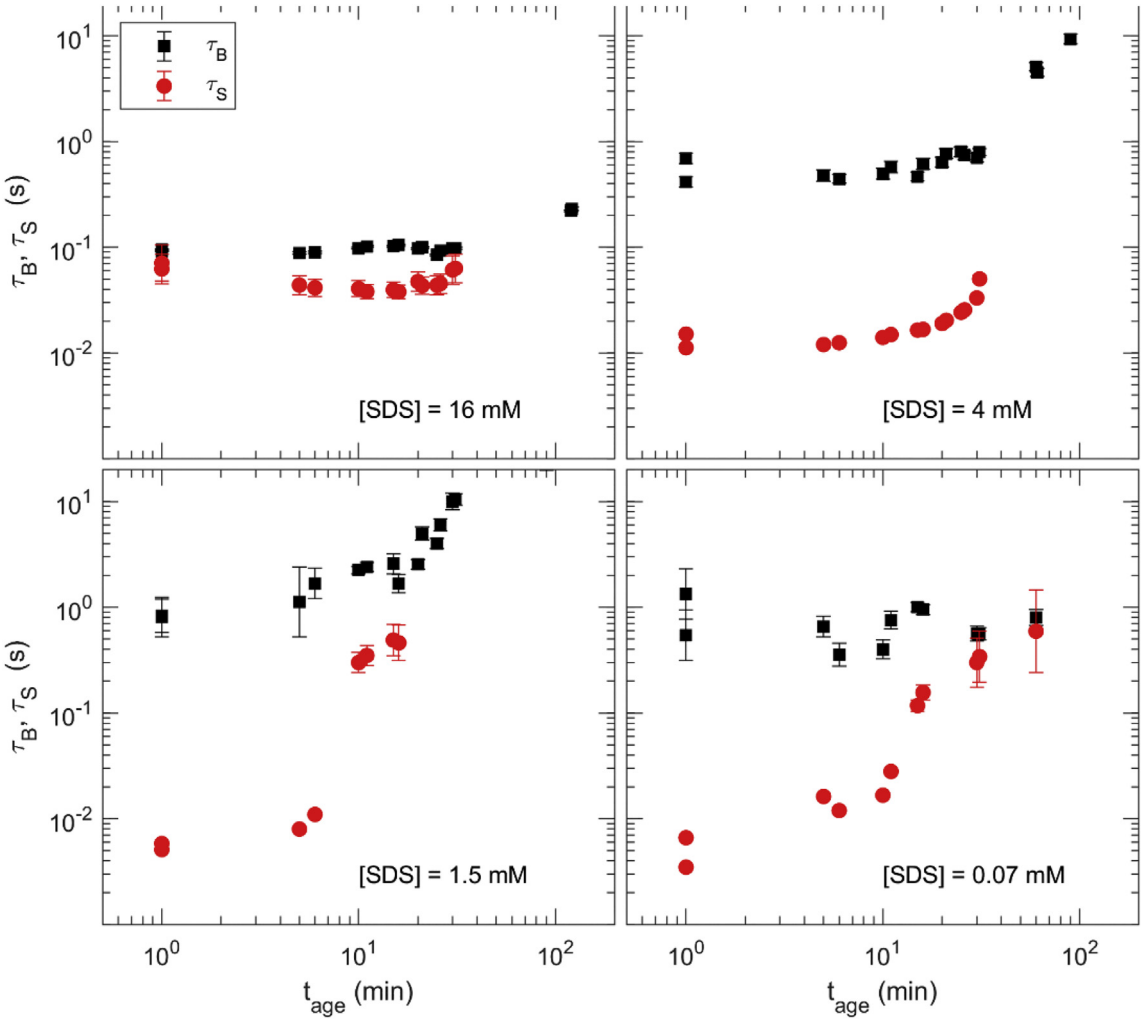


**Fig. 6.** Evolution of Brownian decay time $\tau_B$ and shear decay time $\tau_s$ as a function of the ageing time of the emulsion, for emulsions stabilized by different [SDS] content. At long ageing times, $\tau_s$ cannot be precisely determined once Brownian diffusion dominates and $\tau_B > \tau_s$; the fit yields a value of $\tau_s$ that lies outside of the axis's limits.

quantitatively, while models describe in detail what happens in "creamed" dense emulsions. The analysis we propose here wants to fill this gap.

From the model used to fit DWS correlation functions we obtained values for $\tau_B$ and $\tau_S$ which encode respectively Brownian dynamics and heterogeneous ballistic motions in the sample. The former is quite well understood, being driven by thermal fluctuations, with some corrections in dense emulsions to take into account effects due to drop packing [31]. On the contrary, for ballistic heterogeneous dynamics we cannot apply here directly the interpretation derived in the literature [33] which was developed to describe the motion of tracers in a viscous flow with shear rates well-defined, even if the case of space variation was considered. In the case of interest to us, scattering centres are the drops of an emulsion during creaming or sedimentation. Thus, we must consider the different velocities of individual drops in an otherwise static fluid matrix. Following the line of reasoning of [33] - for inhomogeneous velocity gradients - $\Gamma^2$ must be averaged over the whole volume probed, thus $\Gamma$ is replaced by $\bar{\Gamma} = \sqrt{\langle \Gamma^2 \rangle}$. It is important to underline that "The mean free path, sets the length scale over which $\bar{\Gamma}$ is measured".

The dephasing of a photon path undergoing n scattering events $\Phi^n(t)$ as defined e.g. in Eq. (1) of [33], is given by the sum of n terms of the type $\boldsymbol{k_i} \cdot [\boldsymbol{\Delta v_i}\, t]$ where $\boldsymbol{\Delta v_i}$represents the velocity difference between scattering centres i + 1 and $i$ and $\boldsymbol{k_i}$ is the impinging wavevector for the

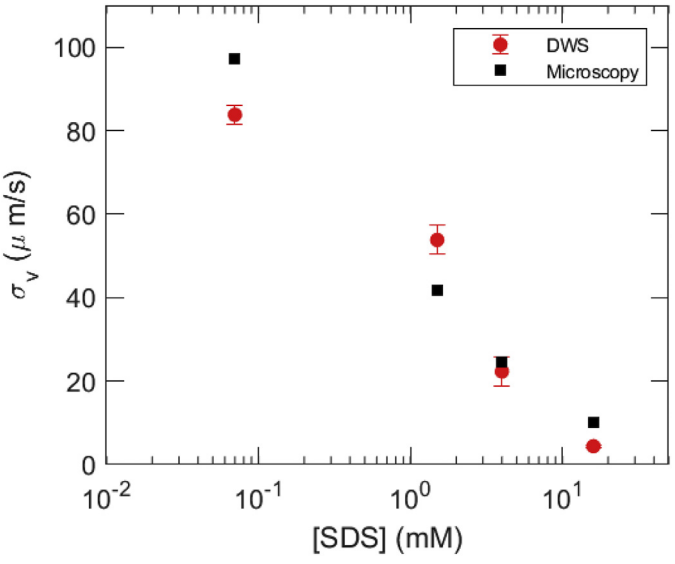


**Fig. 7.** Comparison of the standard deviation of velocities, $\sigma_v$, measured at early times as a function of surfactant content [SDS] by DWS (red circles), with the same quantity obtained from the Hadamard-Rybczynski relation (Eq. (1)), assuming the drop size distribution measured by microscopy (black squares).

*i*-th scattering event. The temporal evolution of these dephasing terms, after appropriate 3D averaging, and weighted sum over path lengths, governs the decay of the heterodyne correlation function. Hence it is natural to introduce the root mean square value of the difference of creaming velocities $\bar{v} = \sqrt{\langle(\Delta v)^2\rangle}$ and to identify it with $\bar{v} = \bar{\Gamma} \cdot l^*$.

We can then use the relation $\langle(\Delta v)^2\rangle = 2\,\sigma_v^2$ and Eq. (8) to directly obtain the relation between $\tau_S$ and the variance of velocity distribution:

$$\sigma_v^2 = 15(\tau_s k_0)^{-2} \tag{10}$$

As stated, this analysis is sensitive to velocity differences between scattering centres, and not their average velocities.

The results of this analysis are reported as a function of surfactant content in Fig. 7 (red points) and compared with the values obtained by microscopy (black squares, data obtained from the Hadamard-Rybczynski relation, Eq. (1)). The agreement between the results of such very different techniques is satisfactory, thus confirming the validity of the proposed analysis scheme for DWS in which we relate the decay of correlation functions to the variance of the velocities of the scattering centres. This agrees with the classical results by Bicout and co-authors [34,35] reported in the Introduction, and is also confirmed by recent experiments on dense granular media fluidized by mechanical agitation [52].

We note in passing that the same analysis scheme could be also applied to the perfectly equivalent case of an emulsion subject to sedimentation.

It is important to pinpoint that in emulsions, the quantification of drop velocity difference is important for two reasons: firstly, in itself, this parameter affects the probability of drop-drop collisions during the creaming process, which is a pre-requisite for coalescence events. This is particularly important for the less-stable emulsions, in which coalescence events happen on the same time scale as creaming, with a possible cross-correlation effect by which coalesced drops rise much faster hence determining chains of events. Besides this, and even for much more stable emulsions in which coalescence is not so rapid, the spread of the velocity distribution is linked to the drop size distribution $f(R)$, since the velocity of each individual drop is related to its size (and marginally to its coverage by surfactants, as explained earlier).

In fact, by the Hadamard Rybczynski relation, Eq. (1), we can link the variance of creaming velocities to the 2.nd and 4.th moments of drop radii distribution, namely $\langle R^2\rangle$ and $\langle R^4\rangle$:

$$\sigma_v^2 \overset{\text{def}}{=} \langle v^2\rangle - \langle v\rangle^2 = \left(\frac{2\,\Delta\rho g}{3\eta}\left(\frac{\eta+\eta'}{2\eta+3\eta'}\right)\right)^2 \left[\langle R^4\rangle - \langle R^2\rangle^2\right] \tag{11}$$

These moments are defined as $<R^n> = \int_0^\infty R^n f(R)\,dR$ $(n = 2,4)$ not to be confused with the corresponding central moments, which are defined around the mean value. The practical result is that both the width and the average value of the drop size distribution contribute to the variance of creaming velocities.

It is not surprising that for the emulsions with increasing surfactant content, on average the drop radii decrease as consistently shown by the analysis of photon transport length $l^*$ and confirmed by direct microscopic observation.

As mentioned, hydrodynamic correlation can be important both in accelerating or in retarding the creaming / sedimentation processes; foams and concentrated emulsions in mechanical equilibrium may be modelled as an assembly of soft elastic interacting particles [53]. Neglecting correlations seems questionable in general, however in some cases the two effects can partly cancel each other as suggested by the results obtained by Xue and co-authors [11] who investigated Brownian diffusion and sedimentation of hard spheres by DWS experiments on a suspension of polystyrene latex particles quite monodisperse in size ($15.5 \pm 0.2\ \mu m$) suspended in a bearing flow of water. In their case, the particles being identical, variance might only arise because of hydrodynamic effects. They found that, at least for such monodisperse sample, the variance of sedimentation velocities vanishes for particle concentrations larger than 0.4 thus implying that hydrodynamic effects do not significantly contribute to velocity variance.

To extend our tests on the applicability of the procedures proposed here, we also characterized the creaming process in other dodecane-in-water emulsions stabilized by SDS at the concentration 4 *mM*, which are formed by larger drops as they are produced in milder conditions by repeated syringe extrusion. In this case, a broad distribution of creaming velocities, linked to high polydispersity of the drop size distribution, is expected. In these cases, DWS investigation faces relevant challenges: a) large drops means large values of $l^*$; consequently, DWS correlation functions are severely affected by the finite sample size; b) the creaming process is fast, imposing limits on the total measurement time and therefore on the accuracy of correlation functions. Results from macroscopic imaging and DWS on these emulsions are reported as Supplementary information, Fig. S2 and S3 respectively. Briefly, we observe a constant correlation between $l^*$, and thus the average radius $\langle R\rangle$ and the average creaming velocity measured by macroscopic imaging. This is expected basing on the relation between creaming velocity and radius. Furthermore, the quantity $1/\tau_S$ proportional to the width of the velocity distribution $\sigma_v$, decreases with increasing emulsification rate, indicating that emulsions with narrower size distributions are produced when higher emulsification energy is employed. These results are not surprising in themselves, but further corroborate the validity of the proposed analysis scheme.

The same analysis could also be applied to the results of DWS experiments performed in preparation of future experiments on emulsions in microgravity to be performed on ESA's *Soft Matter Dynamics* (SMD) facility onboard of the Columbus module of the ISS. In SMD, emulsions are produced directly in the measurement cell, which incorporates a piston which can be activated by applying an oscillating magnetic field. The very strict constraints inherent space experiments imply that sample cells are very limited in size, currently of the order of one cubic cm.The occurrence of emulsions whose $l^*$ is comparable to the sample size, which we expect to be likely given the small sample size and the low energy involved in piston emulsification, demands an analysis of DWS data that accounts for finite sample size effects, such as the one presented here.

In preparation for such experiments, we performed preliminary DWS experiments on an “elegant breadboard” i.e. on an equivalent to the SMD apparatus available on ground at Airbus, Friedrichshafen (DE). Preliminary data collected on different emulsions, an example of which is shown in the Supplementary Information, fig. S4, invariably demonstrated the inapplicability of the standard model of Eq. (5) and (6), and demand for the type of analysis described here.

Finally, the task of characterizing morphology and dynamics of emulsions is difficult because of the number of interactions occurring, of polydispersity of drop size, and of the wide temporal scales interested by the dynamics, from the sudden coalescence events to the very slow Ostwald Ripening processes. Therefore, DWS alone can give only a partial picture that could be usefully complement by confocal microscopy, which could extend the investigation to address critical issues such as depth-dependent caging effects or drop aggregation and coalescence. Information from microscopy could be analysed either by algorithms of Multiple Particle Tracking (MPT) [4,54] operating in the direct space, or by Differential Dynamic Microscopy (DDM) in the reciprocal space, which offers a more direct link to the results obtained by DWS. DDM is a simple but very powerful method based on optical microscopy and image correlation in Fourier space introduced by Cerbino and Trappe [55,56].

## 5. Conclusions and perspectives

In conclusion, after reviewing current trends and some selected recent results obtained by DWS on emulsions, we proposed here a novel

scheme of analysis for DWS by which, starting from a realistic simulation of the distribution of optical path lengths that accounts for the real sample cell, we arrive by Eq. (10) to measure the variance of the velocity distribution of the scattering centres. The quantification of velocity difference in the motion of the drops of an emulsion is important, as this might govern the frequency of drop-drop collisions and subsequent coalescence events in not too stable emulsions.

Furthermore, the variance of velocities given by Eq. (10) can be indicative of the width of radii distribution: when the dominant dynamics is gravity – driven, such as in emulsions subject to sedimentation or creaming, this distribution is related - via the Hadamard-Rybczynski relation (Eq. (1)) possibly with the corrections proposed by Levich (Eq. (2)) - to the 2nd and 4th moments of drop size distribution. It is unfortunate however that only a combination of these two is accessible, while it would be desirable to directly access the two moments separately. We suggest here that a different optical setup, taking advantage of the strong heterodyning limit, could directly measure drop velocities (as opposite to velocity differences) and, from these, get more direct information. Future investigations shall be directed towards this aim.

The proposed analysis has been applied here to a set of model emulsions formed by dodecane in water stabilized by SDS, focusing on the early stages dominated by creaming. At difference with the trends observed by DWS at later stages, this novel analysis shows an interesting dependence of drop radii from surfactant content, which disappears at later times when creaming has completed its course.

It is evident that to further proceed in the understanding of the mechanisms (de)stabilizing emulsions, these early stages dominated by gravity are very important and the extension of DWS to these is expected to represent an important step forward for future research. For instance, the role of surfactant is not completely understood even for such simple model systems. A naïve analysis of the Levich corrections to the Hadamard- Rybczynski relation for creaming velocity seems to suggest that surfactant might contribute only minor corrections in the model emulsion investigated here, modulating at most the 16% difference between the velocity of a rigid sphere and of a drop of dodecane. On the contrary, it is clear that surfactants play a key role in the drop dynamics, as demonstrated by the onset of the peak observed when plotting as a function of surfactant content both single drop dilational viscosity and DWS relaxation times on emulsions of the same composition and measured after long ageing, as previously reported by us in [6]. It is expected that in the near future novel DWS experiments shall shed some light on the role of surfactants, and on the interplay with hydrodynamic correlations and caging effects.

Also, it is expected that the combination of confocal microscopy, interpreted either by Multiple Particle Tracking or by Differential Dynamic Microscopy, joint with results from DWS experiments on the same emulsions, could provide a more complete characterization of drop size distributions, and access heterogeneous dynamics such as drop coalescence and aggregation. This is particularly important for the case of dilute emulsions, for which the link between $l^*$ and $R$ is questionable, as the drop-drop separation must also be considered. For these, complementary information from microscopy observation is anticipated to be necessary.

Finally, the analysis procedures proposed here to model DWS results are also motivated by future investigations on emulsions in microgravity planned to be performed on ESA's *Soft Matter Dynamics* (SMD) facility onboard of the Columbus module of the ISS.

## Authors contribution

CL designed the research, after discussions with FJ, LL and RF.
LV, OD, MMR, SF, and CL performed the DWS experiments.
CL cured Mont Carlo simulations.
LV, OD, and CL analysed DWS results.
OD and SF cured the microimaging experiments.
LL and RF modelled interfacial effects.
CL wrote the manuscript with help from OD, VL and LL.
All the authors commented on the manuscript.

## Declaration of Competing Interest

None.

## Acknowledgments

The authors wish to acknowledge the financial support of the European Space Agency, within the MAP project “Emulsion Dynamics and Droplet Interfaces - EDDI”, (ESA Contract n. 4000128643/19/NL/PG) and the “Foams and Emulsions Technology” Topical Team.

The help of Robert Sütterlin, Airbus, Friedrichshafen for the access to the “Elegant Breadboard” is gratefully acknowledged.

## Appendix A. Supplementary data

Supplementary data to this article can be found online at https://doi.org/10.1016/j.cis.2020.102341.

## References

[1] Weitz DA, Pine DJ. Diffusing-wave spectroscopy. In: Brown W, editor. Dyn. Light Scatt. Method Some Appl. Clarendon Press; 1993.
[2] Pine D, Weitz D, Chaikin PM, Herbolzheimer E. Diffusive wave spectroscopy. Phys Rev Lett 1988;60:1134–7.
[3] Badruddoza AZM, MacWilliams SV, Sebben DA, Krasowska M, Beattie D, Durian DJ, et al. Diffusing wave spectroscopy (DWS) methods applied to double emulsions. Curr Opin Colloid Interface Sci 2018;37:74–87. https://doi.org/10.1016/j.cocis.2018.06.006.
[4] Cristofolini L, Orsi D, Isa L. Characterization of the dynamics of interfaces and of interface-dominated systems via spectroscopy and microscopy techniques. Curr Opin Colloid Interface Sci 2018;37:13–32. https://doi.org/10.1016/j.cocis.2018.06.001.
[5] Orsi D, Salerni F, Macaluso E, Santini E, Ravera F, Liggieri L, et al. Diffusing wave spectroscopy for investigating emulsions: I. Instrumental aspects. Colloids Surfaces A Physicochem Eng Asp 2019;580:123574. https://doi.org/10.1016/j.colsurfa.2019.123574.
[6] Salerni F, Orsi D, Santini E, Liggieri L, Ravera F, Cristofolini L. Diffusing wave spectroscopy for investigating emulsions: II. Characterization of a paradigmatic oil-in-water emulsion. Colloids Surfaces A Physicochem Eng Asp 2019;580:123724. https://doi.org/10.1016/j.colsurfa.2019.123724.
[7] Ravera F. Emulsification and emulsion stability: the role of the interfacial properties of the liquid-liquid system. Adv Colloid Interface Sci 2020.
[8] Rondón M, Bouriat P, Lachaise J, Salager J-L. Breaking of water-in-crude oil emulsions. 1. Physicochemical phenomenology of demulsifier action. Energy Fuel 2006;20:1600–4. https://doi.org/10.1021/ef060017o.
[9] Berg JC. An introduction to interfaces and colloids. World Scientific; 2009. https://doi.org/10.1142/7579.
[10] Levich VG. Physicochemical hydrodynamics. Prentice Hall: Englewood Cliffs, NJ; 1962.
[11] Xue J-Z, Herbolzheimer E, Rutgers MA, Russel WB, Chaikin PM. Diffusion, dispersion, and settling of hard spheres. Phys Rev Lett 1992;69:1715–8. https://doi.org/10.1103/PhysRevLett.69.1715.
[12] Mishchuk NA, Sanfeld A, Steinchen A. Interparticle interactions in concentrate water–oil emulsions. Adv Colloid Interface Sci 2004;112:129–57.
[13] Schramm LL. 5. Colloidal Stability. Emuls. foam. suspens. aerosols microscience appl. Wiley-VCH; 2014. p. 163–204.
[14] Dukhin SS, Mishchuk N, Loglio G, Liggieri L, Miller R. Coalescence coupling with flocculation in dilute emulsions within the primary and/or secondary minimum. Adv Colloid Interface Sci 2003;100:47–81.
[15] Binks B, Cho W, Fletcher P. Disjoining pressure isotherms for oil-water-oil emulsion films. Langmuir 1997;13:7180–5.
[16] Llamas S, Santini E, Liggieri L, Salerni F, Orsi D, Cristofolini L, et al. Adsorption of sodium dodecyl sulfate at water-dodecane interface in relation to the oil in water emulsion properties. Langmuir 2018;34.
[17] Goloub T, Pugh RJ. The role of the surfactant head group in the emulsification process: single surfactant systems. J Colloid Interface Sci 2003;257:337–43.
[18] Deminiere B, Colin A, Calderon F, Bibette J. Coarsening due to coalescence and lifetime of concentrated emulsions. Comptes Rendus L Acad Des Sci Ser Ii Fasc C-Chimie 1998;1:163–5.
[19] Liggieri L, Miller R. Relaxation of surfactants adsorption layers at liquid interfaces. Curr Opin Colloid Interface Sci 2010;15:256–63.
[20] Taylor P. Ostwald ripening in emulsions. Adv Colloid Interface Sci 1998;75:107–63. https://doi.org/10.1016/S0001-8686(98)00035-9.
[21] Voorhees PW. The theory of Ostwald ripening. J Stat Phys 1985;38:231–52. https://doi.org/10.1007/BF01017860.

[22] Cantat I, Höhler R. Foams : Structure and dynamics. Oxford University Press; 2013.
[23] Dukhin SS, Kovalchuk VI, Gochev GG, Lotfi M, Krzan M, Malysa K, et al. Dynamics of rear stagnant cap formation at the surface of spherical bubbles rising in surfactant solutions at large Reynolds numbers under conditions of small Marangoni number and slow sorption kinetics. Adv Colloid Interface Sci 2015;222:260–74. https://doi.org/10.1016/j.cis.2014.10.002.
[24] Pawliszak P, Ulaganathan V, Bradshaw-Hajek BH, Manica R, Beattie DA, Krasowska M. Mobile or immobile? Rise velocity of air bubbles in high-purity water. J Phys Chem C 2019. https://doi.org/10.1021/acs.jpcc.9b03526.
[25] Chan DYC, Klaseboer E, Manica R. Film drainage and coalescence between deformable drops and bubbles. Soft Matter 2011;7:2235–64. https://doi.org/10.1039/c0sm00812e.
[26] Zholkovskij EK, Koval'Chuk VI, Dukhin SS, Miller R. Dynamics of rear stagnant cap formation at low Reynolds numbers. 1 Slow sorption kinetics. J Colloid Interface Sci 2000;226:51–9. https://doi.org/10.1006/jcis.2000.6786.
[27] Dukhin SS, Miller R, Loglio G. Physico-chemical hydrodynamics of rising bubbles. In: Moebius D, Miller R, editors. Drops bubbles interfacial reserach (Moebius D., Mill. R., Eds.), Stud. interface sci. vol. 6. Amsterdam: Elsevier; 1998. p. 367–432.
[28] Berne BJ, Pecora R. Dynamic light scattering. New York: Dover; 2000.
[29] Mason TG, Weitz DA. Optical measurements of frequency-dependent linear viscoelastic moduli of complex fluids. Phys Rev Lett 1995;74:1250–3. https://doi.org/10.1103/PhysRevLett.74.1250.
[30] Mason TG. Estimating the viscoelastic moduli of complex fluids using the generalized stokes-Einstein equation. Rheol Acta 2000;39:371–8. https://doi.org/10.1007/s003970000094.
[31] Kim HS, Şenbil N, Zhang C, Scheffold F, Mason TG. Diffusing wave microrheology of highly scattering concentrated monodisperse emulsions. Proc Natl Acad Sci U S A 2019;116:7766–71. https://doi.org/10.1073/pnas.1817029116.
[32] Chowdhury DP, Sorensen CM, Taylor TW, Merklin JF, Lester TW. Application of photon correlation spectroscopy to flowing Brownian motion systems. Appl Optics 1984;23:4149. https://doi.org/10.1364/AO.23.004149.
[33] Wu X-L, Pine DJ, Chaikin PM, Huang JS, Weitz DA. Diffusing-wave spectroscopy in a shear flow. J Opt Soc Am B 1990;7:15. https://doi.org/10.1364/josab.7.000015.
[34] Bicout D, Maynard R. Diffusing wave spectroscopy in inhomogeneous flows. Phys A Stat Mech Appl 1993;199:387–411. https://doi.org/10.1016/0378-4371(93)90056-A.
[35] Bicout D, Maret G. Multiple light scattering in Taylor-Couette flow. Phys A Stat Mech Appl 1994;210:87–112. https://doi.org/10.1016/0378-4371(94)00101-4.
[36] Skipetrov SE, Meglinskiĭ IV. Diffusing-wave spectroscopy in randomly inhomogeneous media with spatially localized scatterer flows. J Exp Theor Phys 1998;86:661–5. https://doi.org/10.1134/1.558523.
[37] Meglinski I, Tuchin VV. Diffusing wave spectroscopy: Application for blood diagnostics. Handb. Coherent-domain opt. Methods. New York, NY: Springer New York; 2013; 149–66. https://doi.org/10.1007/978-1-4614-5176-1_4.
[38] Uhomoibhi JO, Earnshaw JC. Diffusing wave spectroscopy of uniform translational motion. J Phys Condens Matter 2000;12:9591–8. https://doi.org/10.1088/0953-8984/12/46/306.
[39] Doronin A, Radosevich AJ, Backman V, Meglinski I. Two electric field Monte Carlo models of coherent backscattering of polarized light. J Opt Soc Am A 2014;31:2394. https://doi.org/10.1364/JOSAA.31.002394.
[40] Crassous J. Diffusive wave spectroscopy of a random close packing of spheres. Eur Phys J E 2007;23:145–52. https://doi.org/10.1140/epje/i2006-10079-y.
[41] Fahimi Z, Aangenendt FJ, Voudouris P, Mattsson J, Wyss HM. Diffusing-wave spectroscopy in a standard dynamic light scattering setup. Phys Rev E 2017;96:062611. https://doi.org/10.1103/PhysRevE.96.062611.
[42] Hajjarian Z, Nadkarni SK. Evaluation and correction for optical scattering variations in laser speckle rheology of biological fluids. PLoS One 2013;8:6349–61. https://doi.org/10.1371/journal.pone.0065014.
[43] Hajjarian Z, Nadkarni SK. Correction of optical absorption and scattering variations in laser speckle rheology measurements. Opt Express 2014;22:6349. https://doi.org/10.1364/OE.22.006349.
[44] Brake J, Jang M, Yang C. Analyzing the relationship between decorrelation time and tissue thickness in acute rat brain slices using multispeckle diffusing wave spectroscopy. J Opt Soc Am A 2016;33:270–5. https://doi.org/10.1364/JOSAA.33.000270.
[45] Gang H, Krall aH, Weitz DA. Thermal fluctuations of the shapes of droplets in dense and compressed emulsions. Phys Rev E 1995;52:6289–302. https://doi.org/10.1103/PhysRevE.52.6289.
[46] Yoon J, Cardinaux F, Lapointe C, Zhang C, Mason TG, Ahn KH, et al. Brownian dynamics of colloidal microspheres with tunable elastic properties from soft to hard. Colloids Surfaces A Physicochem Eng Asp 2018;546:360–5. https://doi.org/10.1016/j.colsurfa.2018.02.046.
[47] Braibanti M, Kim HS, Şenbil N, Pagenkopp MJ, Mason TG, Scheffold F. The liquid-glass-jamming transition in disordered ionic nanoemulsions. Sci Rep 2017;7:13879. https://doi.org/10.1038/s41598-017-13584-w.
[48] Höhler R, Cohen-Addad S, Durian DJ. Multiple light scattering as a probe of foams and emulsions. Curr Opin Colloid Interface Sci 2014;19:242–52. https://doi.org/10.1016/j.cocis.2014.04.005.
[49] Dixon PK, Durian DJ. Speckle visibility spectroscopy and variable granular fluidization. Phys Rev Lett 2003;90:4. https://doi.org/10.1103/PhysRevLett.90.184302.
[50] Durian DJ. Accuracy of diffusing-wave spectroscopy theories. Phys Rev E 1995;51:3350–8. https://doi.org/10.1103/PhysRevE.51.3350.
[51] Cristofolini L. Matlab central file exchange. www.mathworks.com/matlabcentral/fileexchange/83943-simulate_path_length_distributions; 2020.
[52] Zivkovic V, Biggs MJ, Glass DH, Xie L. Particle dynamics and granular temperatures in dense fluidized beds as revealed by diffusing wave spectroscopy. Adv Powder Technol 2009;20:227–33. https://doi.org/10.1016/j.apt.2009.03.003.
[53] Höhler R, Weaire D. Can liquid foams and emulsions be modeled as packings of soft elastic particles? Adv Colloid Interface Sci 2019;263:19–37. https://doi.org/10.1016/j.cis.2018.11.002.
[54] Mason TG, Weitz DA. Linear viscoelasticity of colloidal hard sphere suspensions near the Glass transition. Phys Rev Lett 1995;75:2770–3. https://doi.org/10.1103/PhysRevLett.75.2770.
[55] Cerbino R, Trappe V. Differential dynamic microscopy: probing wave vector dependent dynamics with a microscope. Phys Rev Lett 2008;100:188102.
[56] Lu PJ, Giavazzi F, Angelini TE, Zaccarelli E, Jargstorff F, Schofield AB, et al. Characterizing concentrated, multiply scattering, and actively driven fluorescent systems with confocal differential dynamic microscopy. Phys Rev Lett 2012;108:218103. https://doi.org/10.1103/PhysRevLett.108.218103.